JACS
JOURNAL OF THE AMERICAN CHEMICAL SOCIETY
Article
pubs.acs.org/JACS

Tip-Directed Synthesis of Multimetallic Nanoparticles

Peng-Cheng Chen,[†] Guoliang Liu,[‡,⊥] Yu Zhou,[†] Keith A. Brown,[‡] Natalia Chernyak,[‡] James L. Hedrick,[§] Shu He,[‡] Zhuang Xie,[‡] Qing-Yuan Lin,[†] Vinayak P. Dravid,[†] Stacy A. O'Neill-Slawecki,[∥] and Chad A. Mirkin*[,†,‡,§]

[†]Department of Materials Science and Engineering, [‡]Department of Chemistry and International Institute for Nanotechnology, and [§]Department of Chemical and Biological Engineering, Northwestern University, Evanston, Illinois 60208, United States
[∥]Advanced Manufacturing Technologies, GlaxoSmithKline, King of Prussia, Pennsylvania 19406, United States

Supporting Information

ABSTRACT: Alloy nanoparticles are important in many fields, including catalysis, plasmonics, and electronics, due to the chemical and physical properties that arise from the interactions between their components. Typically, alloy nanoparticles are made by solution-based synthesis; however, scanning-probe-based methods offer the ability to make and position such structures on surfaces with nanometer-scale resolution. In particular, scanning probe block copolymer lithography (SPBCL), which combines elements of block copolymer lithography with scanning probe techniques, allows one to synthesize nanoparticles with control over particle diameter in the 2−50 nm range. Thus far, single-element structures have been studied in detail, but, in principle, one could make a wide variety of multicomponent systems by controlling the composition of the polymer ink, polymer feature size, and metal precursor concentrations. Indeed, it is possible to use this approach to synthesize alloy nanoparticles comprised of combinations of Au, Ag, Pd, Ni, Co, and Pt. Here, such structures have been made with diameters deliberately tailored in the 10−20 nm range and characterized by STEM and EDS for structural and elemental composition. The catalytic activity of one class of AuPd alloy nanoparticles made via this method was evaluated with respect to the reduction of 4-nitrophenol with $NaBH_4$. In addition to being the first catalytic studies of particles made by SPBCL, these proof-of-concept experiments demonstrate the potential for SPBCL as a new method for studying the fundamental science and potential applications of alloy nanoparticles in areas such as heterogeneous catalysis.

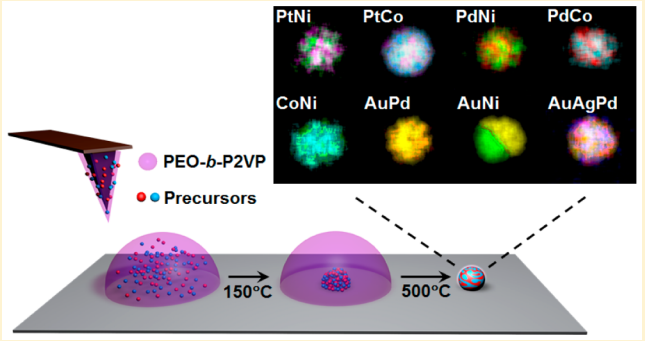

INTRODUCTION

Multimetallic nanoparticles, commonly referred to as alloy nanoparticles, have attracted interest in many areas, including catalysis,[1−5] plasmonics,[6−8] electronics,[9] and magnetics.[10,11] Despite the fact that most alloy nanoparticles are synthesized in solution, the application of alloy nanoparticles often requires their integration on surfaces in a site-specific manner.[12−14] One approach to site-specifically integrating nanoparticles on surfaces involves a synthesis-then-positioning strategy where alloy nanoparticles are first synthesized via wet chemistry[15−17] and then organized on surfaces using lithographically defined templates or more tedious pick-and-place approaches.[18−25] In an alternative paradigm, characterized as precursor-positioning-then-synthesis, metal precursors are physically confined in patterned nanoreactors and subsequently chemically converted into alloy nanoparticles. Examples of nanoreactors include polymer domains defined by block copolymer lithography[26,27] and nanocavities prepared by photolithography[28] or electron-beam lithography.[29]

Recently, we reported a method, termed scanning probe block copolymer lithography (SPBCL),[30−34] that integrates polymer-mediated particle synthesis and molecular printing techniques such as dip-pen nanolithography (DPN)[35−40] and polymer pen lithography (PPL)[41−44] to pattern single nanoparticles on surfaces. The principle behind SPBCL is to first deliver attoliter-scale volumes of metal-coordinated block copolymers to a desired location via scanning probe lithography. These polymer features subsequently function as nanoreactors in which single nanoparticles are locally synthesized.[30,31,45] The nanoparticle size is controlled by the volume and metal loading of the polymer feature, and, in principle, the composition can be controlled by adjusting the types and ratios of metal precursors loaded within the block copolymer nanoreactor.[30−33] Thus far, SPBCL has been generalized to include a broad range of materials such as metals,[31,46] metal oxides,[31,47] and one semiconductor.[32] In addition, the synthesis of a AuAg alloy nanoparticle was effected by patterning Ag and Au precursors simultaneously,[31] which suggests this may be a general approach for preparing alloy

Received: May 18, 2015
Published: July 6, 2015

DOI: 10.1021/jacs.5b05139
J. Am. Chem. Soc. 2015, 137, 9167−9173

nanoparticles, which could be useful for many applications, especially in catalysis. Herein, we study the scope of this approach with Au, Ag, Pd, Ni, Co, and Pt precursors and evaluate the potential for controlling alloy composition for the resulting nanoparticles. Specifically, we find that if the metals are miscible, alloy nanoparticles with a well-defined elemental ratio and even distribution of atoms can be synthesized. If the metals are immiscible, phase-segregated binary particles of well-defined and deliberately controlled size are obtained. We also show that the technique can be used to form ternary alloy nanoparticles consisting of Au, Ag, and Pd, and, as proof-of-concept, we explore the catalytic activity of one class of structures made from Au and Pd with respect to the reduction of 4-nitrophenol with $NaBH_4$.

RESULTS AND DISCUSSION

Previous studies have shown that SPBCL can be used to control the size of single-component nanoparticles by tuning the volume and metal loading of the polymer feature,[30−33] effectively determining the amount of available precursors for forming nanoparticles. However, when considering the synthesis of multicomponent nanoparticles, it is not obvious that a single nanoparticle will be formed. Thus, we initially explore the synthesis of alloy nanoparticles composed of six combinations of transition metals, i.e., AuPd, PtNi, PdNi, PtCo, PdCo, and CoNi, which are widely used for catalysis.[1,2] In a typical experiment (Scheme 1; Supporting Information, Figure S1),

Scheme 1. Polymer-Mediated Tip-Directed Synthesis of Alloy Nanoparticles Using SPBCL[a]

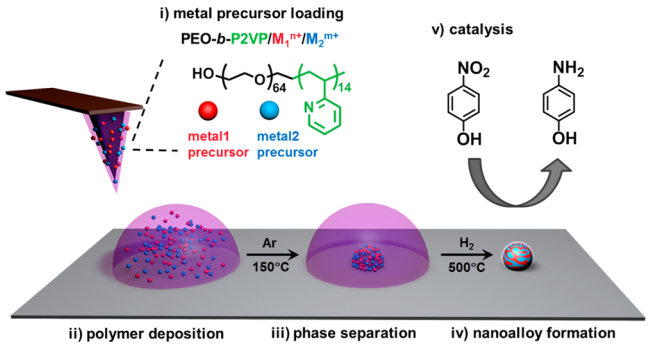

[a]The process consists of five steps: (i) Multiple metal ion precursors are coordinated onto a block copolymer, poly(ethylene oxide)-*block*-poly(2-vinylpyridine) (PEO-*b*-P2VP). (ii) The polymer is cast onto AFM tips or polymer pen arrays and then deposited at desired locations on a substrate. (iii) The substrate is annealed at 150 °C under Ar, allowing the metal ions to aggregate in the polymer nanoreactors. (iv) The substrate is thermally annealed at 500 °C under H_2 to reduce the metal ions and decompose the polymer, forming single alloy nanoparticles in each reactor. (v) The as-prepared alloy nanoparticles are utilized to catalyze the reduction of 4-nitrophenol into 4-aminophenol.

two species of metal precursor (e.g., $HAuCl_4$ and Na_2PdCl_4) were mixed in a solution with a block copolymer, resulting in the metal ions becoming coordinated to the polymer. Here, poly(ethylene oxide)-*block*-poly(2-vinylpyridine) (PEO-*b*-P2VP) was used, as it has been found that the P2VP block coordinates the metal precursors and functions as a carrier to transport metals, while the hydrophilic PEO block facilitates the transport of polymer during patterning experiments.[30] Following ink preparation, an array of atomic force microscopy (AFM) probes was coated with the polymer ink and brought in contact with hydrophobic silicon substrates to deposit the metal-coordinated polymers onto the surface. Figure S1A−C shows typical scanning electron microscopy (SEM) images and an AFM topographical image of the deposited polymer dot arrays. By virtue of performing this patterning with a scanning probe, the pattern of polymer dots can be predefined and controlled through programmed movements of the AFM piezo-scanner (Supporting Information, Figure S2), while the size of each polymer dot is controlled by the tip−substrate contact time and tip withdrawal speed.[48] Following patterning, the polymer dot-coated substrate was annealed at 150 °C to induce the aggregation of various metal precursors inside each dot. Interestingly, single nuclei were observed to form in each polymer dot (Figure S1D). These results suggest that once a nucleus is formed in a polymer nanoreactor, the remaining free metal precursors, regardless of their composition, aggregate onto it due to the lower energy barrier of particle growth than homogeneous nucleation of a new particle.[49] This confined nucleation process ensures the formation of one alloy nanoparticle in each polymer spot. It is important to emphasize that the success of this process is based upon the assumption that homogeneous nucleation is less likely than particle growth, a condition that one would expect to be violated as the reactor becomes larger. Experimentally, we found that nearly all nanoreactors smaller than 350 nm in diameter formed single nanoparticles, but as nanoreactor diameter was increased to 1 μm, nearly all of the nanoreactors formed multiple nuclei (Supporting Information, Figure S3). After the first annealing step, the sample was further annealed at 500 °C to remove the polymer and reduce the metal precursors. Importantly, in all cases studied, the synthesis resulted in the formation of arrays of *single* alloy nanoparticles, suggesting that the precursors conclude the experiment in the same nanoparticle (Figure 1A; Supporting Information, Figure S4).[30,31]

To further confirm the formation of a single alloy nanoparticle in each polymer nanoreactor, we carried out scanning transmission electron microscopy (STEM) and high-resolution transmission electron microscopy (HR-TEM) characterization of nanoparticles synthesized on TEM grids. As shown in STEM images, only one alloy nanoparticle was observed on each site of the square arrays of each bimetallic system (Figure 2; Supporting Information, Figure S5). The inset high-angle annular dark-field (HAADF) STEM images of individual alloy nanoparticles exhibit even contrast, indicating the uniform alloying of each binary system. The morphology of most alloy nanoparticles is quasi-spherical. HR-TEM revealed the crystallinity of one class of AuPd alloy nanoparticles (Figure 1B). Since STEM does not allow for chemical fingerprinting, this characterization was paired with energy-dispersive X-ray spectroscopy (EDS) elemental mapping to investigate the compositional distribution within the alloy nanoparticles. Specifically, EDS mapping confirmed that the nanoparticles were homogeneous mixtures of each binary system (Figure 2; Supporting Information, Figures S6 and S7). This observation can be attributed to the miscibility of these binary metal mixtures.[50] By contrast, we also studied nanoparticles comprised of immiscible metals such as Au and Ni. Notably, STEM imaging of AuNi revealed that Au and Ni were heterogeneously structured in the nanoparticle (Figure 3; Supporting Information, Figure S8), with one region being a Ni subcluster and the other part being a Au subcluster. The brightness contrast between Au and Ni in the STEM image is

DOI: 10.1021/jacs.5b05139
J. Am. Chem. Soc. 2015, 137, 9167−9173

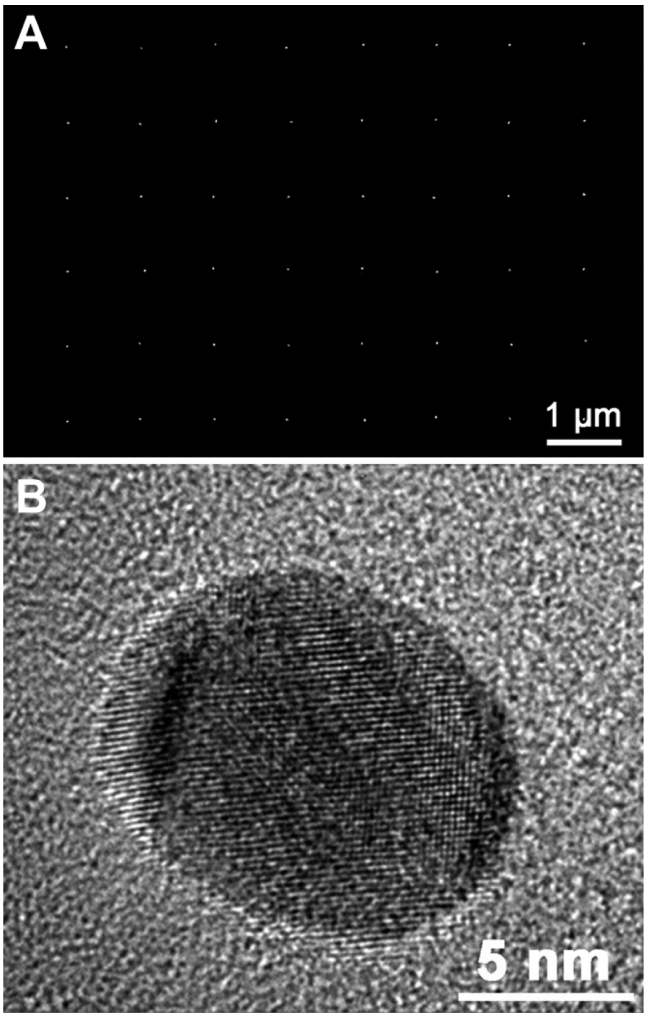

Figure 1. (A) SEM image of a SPBCL-generated AuPd alloy nanoparticle array on a Si substrate. (B) HRTEM image showing that the AuPd nanoparticle is crystalline.

attributed to atomic number contrast. EDS elemental mapping also confirmed the formation of a phase-separated nanoparticle. This phenomenon can be understood by considering the immiscibility of Au and Ni, which form two phases at 500 °C.[50] In addition to bimetallic nanoparticles, arrays of single trimetallic nanoparticles were also synthesized by formulating an ink with PEO-*b*-P2VP and three precursors (i.e., $HAuCl_4$, Na_2PdCl_4, and $AgNO_3$) for SPBCL (Figure 4). The three elements employed here are miscible at arbitrary compositions,[50] which is validated by the EDS elemental mapping of AuAgPd nanoparticles.

The size of SPBCL nanoparticles can be specified by controlling the amount of available precursors for forming nanoparticles.[30−33] In a similar vein, the compositions of SPBCL alloy nanoparticles can, in principle, be controlled by tuning the amount of each constituent metal precursor. To test this compositional control, AuPd and PtNi alloy nanoparticles were synthesized using nine ink solutions with different metal loading ratios. After these inks were patterned and subjected to heat treatment, the resulting alloy nanoparticles were examined using EDS. As shown in Figure 5, the composition of each alloy nanoparticle was within error of the ratio of precursors in the original ink composition, with a standard deviation of less than 10%. Importantly, this result is not *a priori* obvious, since different metals coordinate to PEO-*b*-P2VP with different affinities. We rationalize that the ink loading composition is reproduced in the nanoparticles due to the fact that the vast majority of coordination sites are not occupied, thus mitigating the effects of competitive binding of metal precursors. As a result, the size and composition of alloy nanoparticles are determined exclusively by the polymer feature and ink formulation. It is important to emphasize that this remarkable compositional uniformity of SPBCL alloy nanoparticles is independent of the miscibility of elements. Generally, it is difficult to use wet chemistry to synthesize multimetallic nanoparticles composed of immiscible metals with narrow size and composition distributions.[15−17]

Alloy nanoparticles have been widely studied for applications in catalysis.[1,2,15−17] For example, it has been demonstrated that AuPd alloy nanoparticles exhibit superior activity as compared with nanoparticles composed of Au or Pd alone for many chemical reactions, including the reduction of 4-nitrophenol (4-NP).[51,52] While we have shown that alloy nanoparticles of this kind can be synthesized by SPBCL, it remains to be seen whether these particles are catalytically active and possess the predicted enhanced activity. In particular, one could expect that the annealing process could leave a carbon-rich residue that blocks active sites and prevents activity. To examine the catalytic activity of nanoparticles formed by SPBCL, polymer pen lithography (PPL) was used to synthesize centimeter-scale arrays of nanoparticles (Supporting Information, Figure S9). In particular, arrays of Au, Pd, and AuPd nanoparticles were used to catalyze the reduction of 4-NP with $NaBH_4$ (Figure 6). While all samples with nanoparticles exhibited significantly higher activity than the control samples prepared with inks containing just PEO-*b*-P2VP and no metal precursor, the AuPd alloy nanoparticles showed the highest turnover number (Figure 6C,D), consistent with literature reports of how activity changes with composition.[51,52] Importantly, this result confirms that SPBCL is a viable method for integrating nanoparticle catalysts on a targeted surface.

■ CONCLUSIONS

In summary, we report that SPBCL can be utilized to synthesize a diverse class of alloy nanoparticles (e.g., mixtures of Au, Pd, Ag, Pt, Co, and Ni) in a site-specific manner. Beside the generality of this technique, there are two important advances reported here: (1) that the composition of patterned alloy nanoparticles can be precisely controlled by controlling the ink composition and (2) that the synthesized particles are catalytically active and form high enough quality alloy nanoparticles to display an enhanced catalytic activity. While the reduction of 4-nitrophenol was chosen as a test of the catalytic activity of SPBCL-generated nanoparticles due to its well-studied nature, this work sets the stage for using SPBCL as a novel tool for rapidly synthesizing and screening multicomponent functional nanostructures for catalysis in many important systems.[53]

■ EXPERIMENTAL SECTION

Chemicals. The block copolymer, poly(ethylene oxide)-*block*-poly(2-vinylpyridine) (PEO-*b*-P2VP, M_n = 2.8-*b*-1.5 kg/mol, polydispersity index = 1.11) was purchased from Polymer Source, Inc. and used as received. Metal compounds, $HAuCl_4{\cdot}3H_2O$, Na_2PdCl_4, $H_2PtCl_6{\cdot}6H_2O$, $Co(NO_3)_2{\cdot}6H_2O$, $Ni(NO_3)_2{\cdot}6H_2O$, and $AgNO_3$, were purchased from Sigma-Aldrich, Inc. Hexamethyldisilazane (HMDS), $NaBH_4$ and 4-nitrophenol (4-NP) were purchased from

DOI: 10.1021/jacs.5b05139
J. Am. Chem. Soc. 2015, 137, 9167−9173

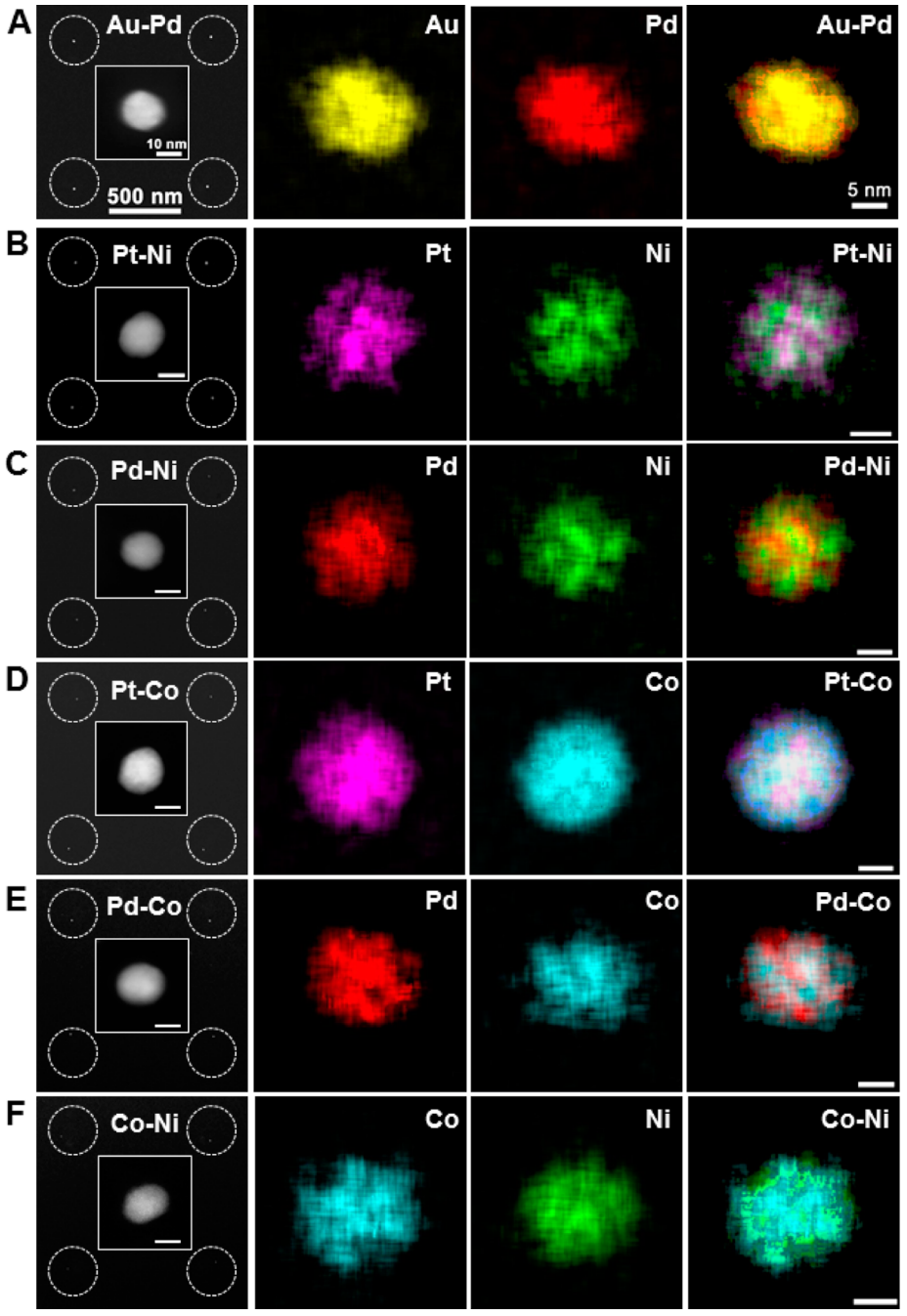

Figure 2. Various 1:1 alloy nanoparticles generated by SPBCL: (A) AuPd, (B) PtNi, (C) PdNi, (D) PtCo, (E) PdCo, and (F) CoNi. First column: HAADF-STEM images of a 2×2 nanoparticle array of each system. Dotted circles highlight the position of nanoparticles as a guide to the eye. The insets are zoomed-in images of single-alloy nanoparticles. Only one nanoparticle was observed at each site. The inset scale bar applies to the insets, and the other applies to all the square array STEM images (see A). Second through fourth columns: EDS elemental mapping of each bimetallic nanoparticle (scale bar = 5 nm).

Sigma-Aldrich, Inc. and used without further purification. DPN 1D pen arrays (type M, no gold coating) were purchased from Nanoink, Inc. TEM grids with hydrophobic silicon nitride support films (film thickness = 15 or 50 nm) were purchased from Ted Pella, Inc., and silicon wafers were purchased from Nova Electronic Materials.

Preparation of Block Copolymer Inks. Polymer inks were prepared by dissolving PEO-*b*-P2VP and various metal compounds in deionized water and then blending them with predetermined molar ratios to achieve inks with specified molar ratios of metal precursors. The resulting solution had a polymer concentration of 5 mg/mL, and the molar ratio of pyridyl group to total metal precursors was 64:1. We expect that the use of a large excess of pyridyl group should lead to a complete complexation of most metal ions from metal precursor salt onto PEO-*b*-P2VP. The pH of the ink solution was lowered to 3−4 by addition of HNO_3 or HCl (acid chosen to match the anion of the metal salt). Inks were stirred for at least 2 days at room temperature prior to use.

SPBCL Patterning Process. DPN pen arrays were dip-coated with inks and allowed to dry under ambient conditions. Following inking, pen arrays were mounted onto an AFM (NScriptor, Nanoink, Inc.) and brought into contact with a substrate to deposit arbitrary arrays of polymer nanoreactors. The patterning process was performed in a chamber at a controlled temperature of 25 °C and relative humidity (RH) of 75%. The size of the polymer nanoreactors was tuned by

DOI: 10.1021/jacs.5b05139
J. Am. Chem. Soc. 2015, 137, 9167−9173

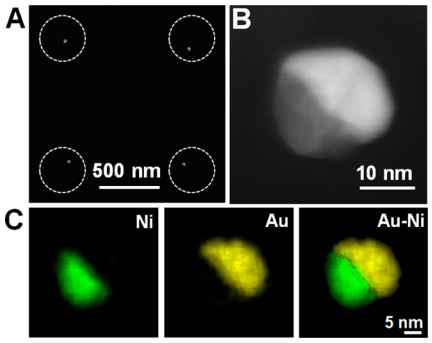

Figure 3. (A) SPBCL pattern of a AuNi nanoparticle array imaged by HAADF-STEM. Dotted circles highlight the position of nanoparticles as a guide to the eye. (B) Enlarged view of a single AuNi nanoparticle. (C) EDS elemental mapping of a single AuNi nanoparticle, showing that the nanoparticle is phase-segregated.

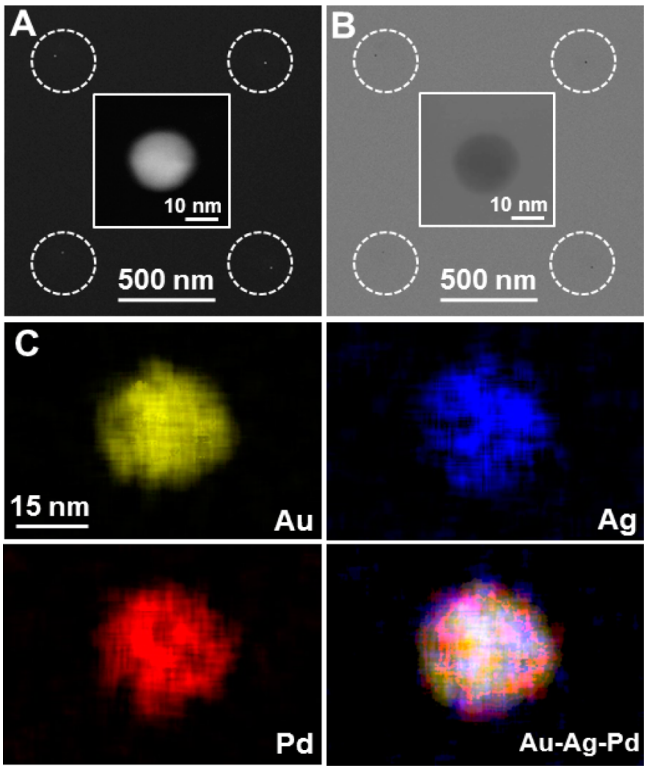

Figure 4. (A) SPBCL pattern of an array of AuAgPd trimetallic nanoparticles imaged by HAADF-STEM and (B) bright-field STEM. (C) EDS elemental mapping of a single AuAgPd nanoparticle. The overlay of Au, Ag, and Pd signals provides evidence for the alloying of these three elements.

adjusting the tip−sample dwell time. Both hydrophobic silicon wafers and hydrophobic TEM grids were used as substrates. Hydrophobic Si wafers were obtained by vapor-coating Si wafers with HMDS for 24 h in a desiccator that contained one vial of a HMDS and hexane mixture (1:1, v/v). In order to convert polymer features into nanoparticles, the substrate was put into a tube furnace and thermally annealed. The heating conditions were programmed as follows: ramp to 150 °C under Ar in 1 h, hold at 150 °C for 48 h, then cool back to room temperature in 1 h, switch the atmosphere into H_2, ramp to 500 °C in 1 h, thermally anneal the substrate at 500 °C for 12 h, and finally cool down to room temperature over 1 h.

PPL Patterning Process. Polymer pen arrays made of PDMS were treated with oxygen plasma (60 W, 2 min) to improve conformity of ink coating. Following this procedure, the pen array

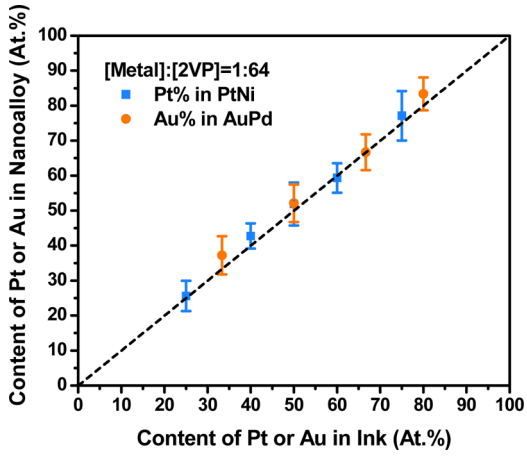

Figure 5. Atomic composition in alloy nanoparticles versus atomic composition in polymer ink. The black dashed line indicates the ideal case. All the data are within variance of the ideal line, with a standard deviation of less than 10%, suggesting that the concentrations of precursors in the ink determine the final nanoparticle composition.

was spin-coated with the ink solution (1000 rpm, 1 min) and allowed to dry in air. The pen array was then mounted on an AFM (XE-150, Park Systems) in a chamber with controlled RH between 90 and 98% at room temperature and brought into contact with a substrate to deposit arrays of polymer nanoreactors. After patterning, the sample was thermally annealed using the aforementioned heating method.

Catalytic Reduction of 4-Nitrophenol. To study the catalytic activity of patterned nanoparticles, 5 μL of aqueous 4-NP solution (1.5 mmol/L) and 5 μL of freshly prepared aqueous $NaBH_4$ solution (750 mmol/L) were successively drop-cast onto a nanoparticle-patterned substrate. The substrate was then stored in a 100% RH environment to minimize water evaporation. After the reaction was allowed to proceed for 3 h at room temperature, both the substrate and the droplet were collected in an Eppendorf tube. Another 140 μL of deionized water was added to rinse the substrate and dilute the droplet. The resulting solution was transferred into a quartz cuvette to collect UV−vis adsorption spectra (Agilent Technologies, Cary 60). The difference in absorption at 400 and 525 nm, respectively, was used to quantify reaction conversion. A contact angle goniometer was used to measure the diameter of droplets in order to normalize the contact area between droplets and different substrates.

Characterization. SEM images were taken with a Hitachi S-4800 field emission scanning electron microscope at an acceleration voltage of 5 kV and a current of 20 μA. AFM measurements were performed on a Dimension Icon (Bruker) to obtain 3D profiles of the polymer nanoreactors. A Hitachi HD-2300 scanning transmission electron microscope was used to image alloy nanoparticles synthesized on TEM grids with 50 nm silicon nitride support films.[54] The bright-field images were recorded using a phase contrast detector, and the dark-field images were taken with a HAADF detector, both at an electron acceleration voltage of 200 kV. The elemental composition of the alloy nanoparticles was studied using dual EDS detectors (Thermo Scientific NSS 2.3) equipped on a HD-2300 STEM with a 200 kV acceleration voltage. EDS spectra were collected to quantify the composition of alloy nanoparticles. EDS mapping was used to visualize the elemental distribution inside alloy nanoparticles. Each EDS map is built on the basis of 30 frames with a pixel size of 0.0625 nm^2 and pixel dwell time of 203 μs. HR-TEM images were taken on a JEOL 2100F transmission electron microscope at an acceleration voltage of 200 kV with alloy nanoparticles prepared on TEM grids with 15 nm silicon nitride support films.

DOI: 10.1021/jacs.5b05139
J. Am. Chem. Soc. 2015, 137, 9167−9173

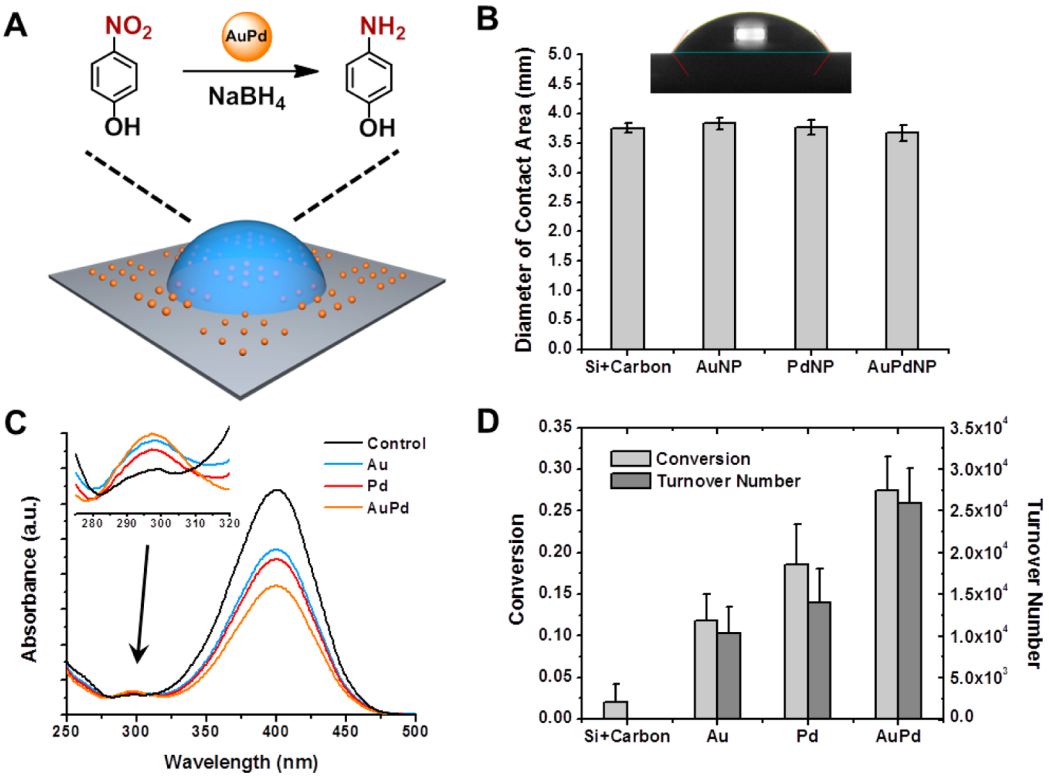

Figure 6. Reduction of 4-nitrophenol catalyzed by a PPL-patterned nanoparticle array. (A) Scheme of the catalysis process. A 10 μL aqueous droplet containing 4-NP and $NaBH_4$ was dispensed onto a nanoparticle array. In the presence of nanoparticles, 4-NP was converted into 4-aminophenol. (B) The diameters of the contact area between droplets and various substrates were determined by a contact angle goniometer. About 0.7 million nanoparticles were covered by each droplet. Inset is a typical photograph of a reactant droplet on a PPL-patterned nanoparticle array. (C) UV−vis absorption spectra of the droplet solution after catalysis was run on different substrates with product and reactant peaks at 296 and 400 nm, respectively. (D) Conversion percentage and turnover number of the reaction catalyzed by control sample (no particles), AuNP (16 ± 2 nm diameter) arrays, PdNP (16 ± 3 nm diameter) arrays, and AuPdNP (16 ± 2 nm diameter) arrays.

■ ASSOCIATED CONTENT

Supporting Information

SEM and AFM images of polymer nanoreactors, SEM images and EDS spectra of various alloy nanoparticles, and dark-field optical microscopy image of large area polymer patterns. The Supporting Information is available free of charge on the ACS Publications website at DOI: 10.1021/jacs.5b05139.

■ AUTHOR INFORMATION

Corresponding Author

*chadnano@northwestern.edu

Present Address

[⊥]G.L.: Department of Chemistry, Virginia Tech, 900 W. Campus Dr., Blacksburg, VA 24061

Notes

The authors declare no competing financial interest.

■ ACKNOWLEDGMENTS

This material is based upon work supported by the Air Force Office of Scientific Research awards FA9550-12-1-0280 and FA9550-12-1-0141, the National Science Foundation awards DBI-1152139 and DBI-1353682, and GlaxoSmithKline LLC Agreement 100037477. Y.Z. acknowledges support from the Ryan Fellowship at Northwestern University. K.A.B. acknowledges support from Northwestern University's International Institute for Nanotechnology. J.L.H. was supported by the U.S. Department of Defense through the National Defense Science & Engineering Graduate Fellowship (NDSEG) Program. Q.-Y.L. acknowledges support from the Hierarchical Materials Cluster Program Fellowship from Northwestern University. This work made use of the EPIC facility (NUANCE Center-Northwestern University), which has received support from the MRSEC program (NSF DMR-1121262) at the Materials Research Center, the International Institute for Nanotechnology (IIN), and the State of Illinois, through the IIN.

■ REFERENCES

(1) Ferrando, R.; Jellinek, J.; Johnston, R. L. *Chem. Rev.* **2008**, *108*, 845.

(2) Tao, F. *Chem. Soc. Rev.* **2012**, *41*, 7977.

(3) Chen, C.; Kang, Y. J.; Huo, Z. Y.; Zhu, Z. W.; Huang, W. Y.; Xin, H. L. L.; Snyder, J. D.; Li, D. G.; Herron, J. A.; Mavrikakis, M.; Chi, M. F.; More, K. L.; Li, Y. D.; Markovic, N. M.; Somorjai, G. A.; Yang, P. D.; Stamenkovic, V. R. *Science* **2014**, *343*, 1339.

(4) Chen, G. X.; Zhao, Y.; Fu, G.; Duchesne, P. N.; Gu, L.; Zheng, Y. P.; Weng, X. F.; Chen, M. S.; Zhang, P.; Pao, C. W.; Lee, J. F.; Zheng, N. F. *Science* **2014**, *344*, 495.

(5) Choi, S. I.; Xie, S. F.; Shao, M. H.; Odell, J. H.; Lu, N.; Peng, H. C.; Protsailo, L.; Guerrero, S.; Park, J. H.; Xia, X. H.; Wang, J. G.; Kim, M. J.; Xia, Y. N. *Nano Lett.* **2013**, *13*, 3420.

(6) Cortie, M. B.; McDonagh, A. M. *Chem. Rev.* **2011**, *111*, 3713.

(7) Gordon, T. R.; Schaak, R. E. *Chem. Mater.* **2014**, *26*, 5900.

(8) Qian, Z.; Park, S.-J. *Chem. Mater.* **2014**, *26*, 6172.

(9) Shipway, A. N.; Katz, E.; Willner, I. *ChemPhysChem* **2000**, *1*, 18.

(10) Alloyeau, D.; Ricolleau, C.; Mottet, C.; Oikawa, T.; Langlois, C.; Le Bouar, Y.; Braidy, N.; Loiseau, A. *Nat. Mater.* **2009**, *8*, 940.

(11) Sun, S. H. *Adv. Mater.* **2006**, *18*, 393.

DOI: 10.1021/jacs.5b05139
J. Am. Chem. Soc. 2015, 137, 9167−9173

(12) Hyun, J. K.; Lauhon, L. J. *Nano Lett.* **2011**, *11*, 2731.
(13) Grunes, J.; Zhu, J.; Anderson, E. A.; Somorjai, G. A. *J. Phys. Chem. B* **2002**, *106*, 11463.
(14) Eggenhuisen, T. M.; Friedrich, H.; Nudelman, F.; Zecevic, J.; Sommerdijk, N. A. J. M.; de Jongh, P. E.; de Jong, K. P. *Chem. Mater.* **2013**, *25*, 890.
(15) Sankar, M.; Dimitratos, N.; Miedziak, P. J.; Wells, P. P.; Kiely, C. J.; Hutchings, G. J. *Chem. Soc. Rev.* **2012**, *41*, 8099.
(16) Wang, D. S.; Li, Y. D. *Adv. Mater.* **2011**, *23*, 1044.
(17) Wang, D. S.; Li, Y. D. *J. Am. Chem. Soc.* **2010**, *132*, 6280.
(18) Cheng, W. L.; Park, N. Y.; Walter, M. T.; Hartman, M. R.; Luo, D. *Nat. Nanotechnol.* **2008**, *3*, 682.
(19) Gong, X. *RSC Adv.* **2014**, *4*, 54494.
(20) Kraus, T.; Malaquin, L.; Schmid, H.; Riess, W.; Spencer, N. D.; Wolf, H. *Nat. Nanotechnol.* **2007**, *2*, 570.
(21) Zhou, Y.; Zhou, X. Z.; Park, D. J.; Torabi, K.; Brown, K. A.; Jones, M. R.; Zhang, C.; Schatz, G. C.; Mirkin, C. A. *Nano Lett.* **2014**, *14*, 2157.
(22) Hung, S. C.; Nafday, O. A.; Haaheim, J. R.; Ren, F.; Chi, G. C.; Pearton, S. J. *J. Phys. Chem. C* **2010**, *114*, 9672.
(23) Wang, W. C. M.; Stoltenberg, R. M.; Liu, S. H.; Bao, Z. N. *ACS Nano* **2008**, *2*, 2135.
(24) Gilles, S.; Tuchscherer, A.; Lang, H.; Simon, U. *J. Colloid Interface Sci.* **2013**, *406*, 256.
(25) Guo, Q. J.; Teng, X. W.; Rahman, S.; Yang, H. *J. Am. Chem. Soc.* **2003**, *125*, 630.
(26) Mun, J. H.; Chang, Y. H.; Shin, D. O.; Yoon, J. M.; Choi, D. S.; Lee, K. M.; Kim, J. Y.; Cha, S. K.; Lee, J. Y.; Jeong, J. R.; Kim, Y. H.; Kim, S. O. *Nano Lett.* **2013**, *13*, 5720.
(27) Ethirajan, A.; Wiedwald, U.; Boyen, H. G.; Kern, B.; Han, L. Y.; Klimmer, A.; Weigl, F.; Kastle, G.; Ziemann, P.; Fauth, K.; Cai, J.; Behm, R. J.; Romanyuk, A.; Oelhafen, P.; Walther, P.; Biskupek, J.; Kaiser, U. *Adv. Mater.* **2007**, *19*, 406.
(28) Konig, D.; Richter, K.; Siegel, A.; Mudring, A. V.; Ludwig, A. *Adv. Funct. Mater.* **2014**, *24*, 2049.
(29) Javey, A.; Dai, H. J. *J. Am. Chem. Soc.* **2005**, *127*, 11942.
(30) Chai, J. A.; Huo, F. W.; Zheng, Z. J.; Giam, L. R.; Shim, W.; Mirkin, C. A. *Proc. Natl. Acad. Sci. U.S.A.* **2010**, *107*, 20202.
(31) Liu, G. L.; Eichelsdoerfer, D. J.; Rasin, B.; Zhou, Y.; Brown, K. A.; Liao, X.; Mirkin, C. A. *Proc. Natl. Acad. Sci. U.S.A.* **2013**, *110*, 887.
(32) Giam, L. R.; He, S.; Horwitz, N. E.; Eichelsdoerfer, D. J.; Chai, J. N.; Zheng, Z. J.; Kim, D.; Shim, W.; Mirkin, C. A. *Nano Lett.* **2012**, *12*, 1022.
(33) Liu, G. L.; Zhou, Y.; Banga, R. S.; Boya, R.; Brown, K. A.; Chipre, A. J.; Nguyen, S. T.; Mirkin, C. A. *Chem. Sci.* **2013**, *4*, 2093.
(34) Chai, J. A.; Wong, L. S.; Giam, L.; Mirkin, C. A. *Proc. Natl. Acad. Sci. U.S.A.* **2011**, *108*, 19521.
(35) Piner, R. D.; Zhu, J.; Xu, F.; Hong, S. H.; Mirkin, C. A. *Science* **1999**, *283*, 661.
(36) O'Connell, C. D.; Higgins, M. J.; Marusic, D.; Moulton, S. E.; Wallace, G. G. *Langmuir* **2014**, *30*, 2712.
(37) Brown, K. A.; Eichelsdoerfer, D. J.; Liao, X.; He, S.; Mirkin, C. A. *Front. Phys.* **2014**, *9*, 385.
(38) Zhong, J.; Sun, G.; He, D. *Nanoscale* **2014**, *6*, 12217.
(39) Hernandez-Santana, A.; Irvine, E.; Faulds, K.; Graham, D. *Chem. Sci.* **2011**, *2*, 211.
(40) Ielasi, F. S.; Hirtz, M.; Sekula-Neuner, S.; Laue, T.; Fuchs, H.; Willaert, R. G. *J. Am. Chem. Soc.* **2015**, *137*, 154.
(41) Huo, F. W.; Zheng, Z. J.; Zheng, G. F.; Giam, L. R.; Zhang, H.; Mirkin, C. A. *Science* **2008**, *321*, 1658.
(42) Zhou, Y.; Xie, Z.; Brown, K. A.; Park, D. J.; Zhou, X.; Chen, P.-C.; Hirtz, M.; Lin, Q.-Y.; Dravid, V. P.; Schatz, G. C.; Zheng, Z.; Mirkin, C. A. *Small* **2015**, *11*, 913.
(43) Brown, K. A.; Eichelsdoerfer, D. J.; Shim, W.; Rasin, B.; Radha, B.; Liao, X.; Schmucker, A. L.; Liu, G. L.; Mirkin, C. A. *Proc. Natl. Acad. Sci. U.S.A.* **2013**, *110*, 12921.
(44) Giam, L. R.; Massich, M. D.; Hao, L. L.; Wong, L. S.; Mader, C. C.; Mirkin, C. A. *Proc. Natl. Acad. Sci. U.S.A.* **2012**, *109*, 4377.
(45) Chai, J.; Liao, X.; Giam, L. R.; Mirkin, C. A. *J. Am. Chem. Soc.* **2012**, *134*, 158.
(46) Wu, J.; Zan, X. L.; Li, S. Z.; Liu, Y. Y.; Cui, C. L.; Zou, B. H.; Zhang, W. N.; Xu, H. B.; Duan, H. W.; Tian, D. B.; Huang, W.; Huo, F. W. *Nanoscale* **2014**, *6*, 749.
(47) Smetana, A. B.; Pacley, S.; Boeckl, J.; Adamczyk, P.; Nettikadan, S. *J. Mater. Chem. C* **2013**, *1*, 1798.
(48) Eichelsdoerfer, D. J.; Brown, K. A.; Mirkin, C. A. *Soft Matter* **2014**, *10*, 5603.
(49) Hoyt, J. J. *Phase Transformations*; McMaster Innovation Press: Hamilton, Canada, 2011.
(50) Baker, H., Ed. *Alloy Phase Diagrams*; ASM International: Materials Park, OH, 1992; Vol.3.
(51) Shi, L. H.; Wang, A. Q.; Zhang, T.; Zhang, B. S.; Su, D. S.; Li, H. Q.; Song, Y. J. *J. Phys. Chem. C* **2013**, *117*, 12526.
(52) Kaiser, J.; Leppert, L.; Welz, H.; Polzer, F.; Wunder, S.; Wanderka, N.; Albrecht, M.; Lunkenbein, T.; Breu, J.; Kummel, S.; Lu, Y.; Ballauff, M. *Phys. Chem. Chem. Phys.* **2012**, *14*, 6487.
(53) Reddington, E.; Sapienza, A.; Gurau, B.; Viswanathan, R.; Sarangapani, S.; Smotkin, E. S.; Mallouk, T. E. *Science* **1998**, *280*, 1735.
(54) Wu, J. S.; Kim, A. M.; Bleher, R.; Myers, B. D.; Marvin, R. G.; Inada, H.; Nakamura, K.; Zhang, X. F.; Roth, E.; Li, S. Y.; Woodruff, T. K.; O'Halloran, T. V.; Dravid, V. P. *Ultramicroscopy* **2013**, *128*, 24.

DOI: 10.1021/jacs.5b05139
J. Am. Chem. Soc. 2015, 137, 9167−9173